Isı Bilimi ve Tekniği Dergisi, 37, 1, 115-125, 2017
J. of Thermal Science and Technology

ISSN 1300-3615

NUMERICAL INVESTIGATION OF THE EFFECT OF BLADE AIRFOILS ON A VERTICAL AXIS WIND TURBINE

Selahaddin Orhan AKANSU*, Toygun DAGDEVİR and Nafiz KAHRAMAN*****
*,**Erciyes University Faculty of Engineering Department of Mechanical Engineering, Kayseri 38039, Turkey,
*akansu@erciyes.edu.tr, **toygun@erciyes.edu.tr
***BFG Teknolojik Araştırmalar Akreditasyon San. ve Tic. Ltd. Şti., Erciyes University,
Erciyes University-Technology Development Zone Kayseri, Turkey, ***nafiz@erciyes.edu.tr
***corresponding author* Tel: +90 (537) 676 1555; Fax: +90 (352) 437 5784; e-mail: toygun@erciyes.edu.tr

(Geliş Tarihi: 11.09.2015, Kabul Tarihi: 11.11.2016)

Abstract: In this study, energy performance and aerodynamic forces acted on a vertical-axis Darrieus wind turbine (VAWT) have been examined by using computational fluid dynamics (CFD) program. Numerical investigation is conducted on a blade fixed pitch VAWT using NACA0021, NACA0015, NACA5520 and Clark-Y airfoils as a blade profile to assess its performance, and these four airfoils were compared with each other's. Numerical simulation is done for two-dimensional unsteady flow around the VAWT model by using Ansys-Fluent program which solves Reynolds averaged Navier-Stokes equations. Considered numerical results, NACA5520 can be employed to generate first movement; in addition, the maximum average power coefficient has been obtained for NACA0021.
Keywords: Vertical axis wind turbine, Airfoil, CFD, Power coefficient.

KANAT PROFİLLERİNİN DİKEY EKSENLİ BİR RÜZGÂR TÜRBİNİ PERFORMANSINA ETKİSİNİN SAYISAL İNCELENMESİ

Özet: Bu çalışmada, dikey eksenli bir rüzgar (DERT) türbini üzerine uygulanan aerodinamik kuvvetler ve enerji performansı, hesaplamalı akışkanlar dinamiği (HAD) programı kullanılarak incelenmiştir. Sayısal araştırma, NACA0021, NACA0015, NACA5520 ve CLARK-Y kanat profillerini kullanmak üzere, rüzgar türbinin performansını değerlendirmek amacıyla gerçekleştirilmiş ve bu dört kanat profili birbirleri ile karşılaştırılmıştır. Ansys-Fluent programı, Reynolds ortalamalı Navier-Stokes denklemlerini çözerek, DERT etrafındaki iki boyutlu kararsız akışı simule etmede kullanılmıştır. Sayısal sonuçlar göz önüne alındığında, NACA5520 kanat profili ilk hareketi sağlamak için kullanılabilirken, buna ek olarak ortalama olarak en yüksek güç katsayısı değeri NACA0021 profilinde elde edilmiştir.
Anahtar Kelimeler: Dikey eksenli rüzgar türbini, Kanat profili, HAD, Güç katsayısı.

NOMENCLATURE

A	rotor swept area [m^2]	TSR	tip speed ratio [-]
c	chord length [m]	U	free wind velocity [m/s]
CD	drag coefficient [-]	β	solid blockage factor [-]
CL	lift coefficient [-]	ε	turbulent dissipation [-]
CP	power coefficient [-]	θ	rotor azimuthal position [°]
CT	torque coefficient [-]	μ	dynamic viscosity [kg/m-s]
D_{rotor}	rotor diameter [m]	μ_e	significant viscosity coefficient [-]
H_{rotor}	rotor height [m]	ρ	air density [kg/m3]
k	turbulent kinetic energy [-]	σ	solidity of the rotor [-]
N	number of blades [-]	σ_k	TKE Prandtl Number [-]
P	wind turbine power output [W]	$\sigma\epsilon$	TDR Prandtl Number [-]
R_{rotor}	rotor radius [m]	ω	rotor angular velocity [rad/s]

INTRODUCTION

Used the wind power for grinding corn and wheat, moving the sailboats for thousand years, from now on it has been used for energy production. Humanity has been undergoing a technological process which from windmills to modern wind power plants. The wind energy was not considered due to the cheapness of fossil fuels, until petrol crises arose in early 1970s. With developments after 1980, the wind power plants in the

America and Europe have become contemporary engineering products in terms of economy, environment and energy. With the introduction of mass production of the wind turbines, as a result of increasing investments in this area and developments on turbine and more and more wind turbines have been planted day by day.

The wind power plants that are previously planted on ground have been planted on seas now, too. On the other hand, the height of wind turbines from ground is a significant parameter to enhance the available power. To investigate this parameter on vertical axis wind turbines, Saeidi et al., (2013) has studied on aerodynamic design and economical evaluation of site specific small vertical axis wind turbines. The economic feasibility of the designed VAWT is integrated in the design procedure to predict annual production of electricity. The results of this study despite the absence of optimization, were sought in aero elastic design at this stage, the designed VAWT can produce 3.1 MWh power annually if it is installed on the mast height of 40 m for a 1.5 kW H_{rotor} VAWT with NACA4415 airfoil sections.

In late 1970s, when small wind turbines were compared with others alternative energies, investment costs decreased and attracted the attention of many people thanks to the effect of developing technology. Between 1979 and 1985 years, the much more 4500 wind power plants made powers ranging from 1 to 25 kW with appropriate government loans. Various properties 1000 number remote-controlled system has established in same period (Bergey, 1997).

The first turbine generated from wind energy was established by Paul la Cour, an outstanding engineer of modern aerodynamic. Since the unit price of electricity is high, the wind power plants capable 55 KW have begun to produce as a result of industrial and technological developments in 1980-1981 (Danish Wind History, 1999).

There are three main parameters often used to characterize the performance of a wind turbine. These parameters are power coefficient, torque coefficient and overall efficiency. Power coefficient is defined as the amount of mechanical power produced by the wind turbine against the total available wind power (Kishore, 2013).

Also, blades' airfoil is a parameter which affects the aerodynamic performance of wind turbines. In this respect, Guleren and Demir (2011) investigated performance analysis of different airfoils for wind turbine blades at low angles of attack. They stated that CLARK Y had the highest performance among other airfoils (EPPLER 625, EPPLER 664, CLARK Y, Eiffel 10, FX 69-PR-281 and NACA Munk M-4) according to C_L and C_L/ C_D values.

Furthermore, some reviews recently have published about assessment of Darrieus VAWT. Enlighten information about configuration and design techniques of VAWTs can be avalible in literature (Tjiu et al (2015), Jin (2015), Bhutta (2012) and Tummala (2016)). Howell et al. (2010) both experimentally and numerically investigated aerodynamic performance of a small VAWT. The numerical study was conducted both 3D and 2D. They combined experimental and computational study of the VAWT. They stated that the 2D simulations revealed a significantly increased performance compared to the 3D simulations and this was shown to be mainly due to the presence of the large tip vortices present in the real turbine and the 3D simulations. And they concluded that the performance is enhanced by having the surface of the turbine roughened below a critical Reynolds number of 30,000. VAWT analyses have been generally conducted with non-dimensional parameters such as power coefficient, torque coefficient and tip speed ratios (TSR).

Nobile et al. (2014) numerically analysed two dimensionally for NACA0018 and NACA0021 on VAWT. The peak power coefficient was obtained at a TSR of 2.75 and 2.50 for NACA0018 and NACA0021, respectively; and they found that the maximum energy extraction of the rotor is upstream with a maximum value at an azimuthal angle of 90º. Furthermore, Nini et al. (2014) investigated performance of vertical axis turbine for 1.52 and 2.5 tip speed ratio on NACA 0021. They suggested that optimal configuration was about 2.5 tip speed ratio. Discrepancy that has emerged between two curves may cause ambiguous parameters in CFD study. Nevertheless, the curve in our study is both closer to experimental study and also complied with literature (Horikiri, 2014).

NUMERICAL ANALYSIS

Computational Fluid Dynamics (CFD) simulations have been commonly used to predict, solve and analyze the problems which involve fluid flows, by using equations and algorithms of fluid mechanics. Critical investigation on fluid mechanics has been carried out with developing the computer, software and advanced numerical algorithm.

The advantage of CFD simulations are to optimize components of models with shorter time and cheaper than experiments. In this section, a 2D simulation of vertical axis wind turbine is investigated. Non-commercial CFD simulation code Fluent 14.5 was used to calculate rotor main kinematic and dynamic characteristics by solving the conservation equations for continuity and momentum. GAMBIT 4.2.6 packed program was used to generate grid structure.

Figure 1 shows a schematic description of the solution methodology. Blade type is determined with solid modeling software, which is an analytical code. In preprocessing, model of the problem is designed and meshing. In post processing, the results which were

obtained from the solution was used to compare with other airfoils.

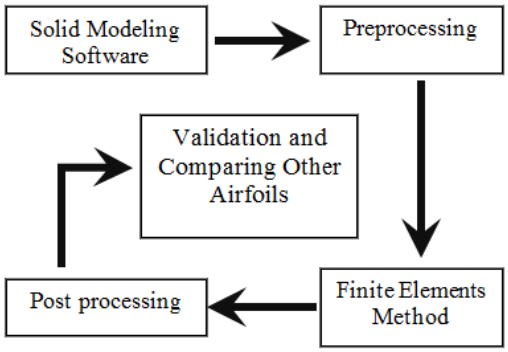

Figure 1. Scheme of the methodology.

The aim of the present work is to simulate and examine the aerodynamic characteristics of a vertical axis wind turbine which is a rotating machine. This study is numerically analysed of the aerodynamic behaviour of a three-bladed Darrieus VAWT operating at different angular velocities for a constant wind speed of 9 m/s, as shown Fig 2. The numerical simulation was carried out by using the Navier-Stokes equation based on the 2D, the fluid was assumed to be incompressible and unsteady flow; density and dynamic viscosity are constant (ρ=1.225 kg/m^3, μ=1.7894x10^{-5} kg/m-s). Sliding mesh method was conducted to simulate behaviour of rotating blades. Residual convergence criterion for x and y velocity, k and ε was set to 1e-6; for continuity was set to 1e-4. This convergence check is adequate to insure the stability of aerodynamic forces upon the airfoils. Each simulation needed to approximately 7-8 tours rotating to reach steady.

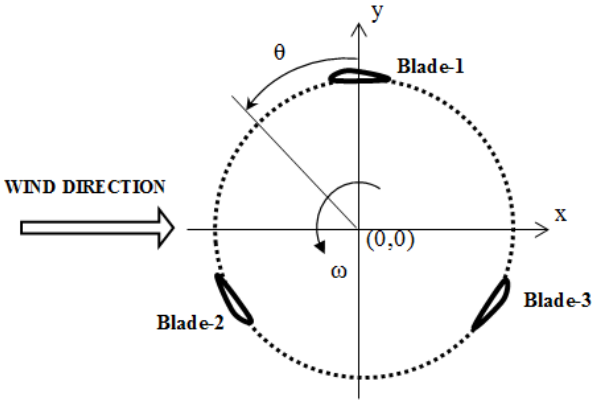

Figure 2. Schematic diagram of numerical system.

For the proposed calculations, the temporal discretization was achieved by setting a physical time step equal to the lapse of time the rotor takes to make a 1˚ rotation. Average torque values were obtained at each 4˚at each simulation. The torque values showed a deviation of less than 2% compared with the equivalent values of the previous period, corresponding to a revolution of 120˚due to rotor three-bladed geometry. According to the conditions in the computation, the continuity equation (1) and momentum equation (2) were shown as below:

$$\frac{\partial \rho}{\partial t} + \frac{\partial (\rho u_j)}{\partial x_j} = 0 \quad (1)$$

$$\frac{\partial (\rho u_i)}{\partial t} + \frac{\partial (\rho u_i u_j)}{\partial x_j} = \frac{\partial \left[\mu_e \left(\frac{\partial u_i}{\partial x_j} + \frac{\partial u_j}{\partial x_i}\right)\right]}{\partial x_j} - \frac{\partial P}{\partial x_j} + S_i \quad (2)$$

x_j is coordinate component, u_i, u_j is the average relative velocity components, μ_e is the significant viscosity coefficient, P is the pressure (Pa), S_i is the generated item. The k-ε turbulence and enhanced wall treatment model was used as the turbulence model, since both Castelli et al. (2011) were recommended and it gives accurate results in flow separation on the walls. Turbulent kinetic energy k (3) and turbulent energy dissipation rate ε (4) were inducted. The constraint equations were expressed as follows:

$$\frac{\partial (\rho k_i)}{\partial t} + \frac{\partial (\rho k u_i)}{\partial x_j} = \frac{\partial}{\partial x_j}\left[\left(\mu + \frac{\mu_t}{\sigma_k}\right)\frac{\partial k}{\partial x_j}\right] + \rho(P_k - \varepsilon) \quad (3)$$

$$\frac{\partial (\rho \varepsilon)}{\partial t} + \frac{\partial (\rho \varepsilon u_i)}{\partial x_j} = \frac{\partial}{\partial x_j}\left[\left(\mu + \frac{\mu_t}{\sigma_\varepsilon}\right)\frac{\partial \varepsilon}{\partial x_j}\right] + \rho \frac{\varepsilon}{k}(C_1 P_k - C_2 \varepsilon) \quad (4)$$

where P_k, the turbulent kinetic energy is generated item, and it is defined as (Yan et al., 2012):

$$P_k = \frac{\mu_t}{\rho}\left(\frac{\partial u_i}{\partial x_j} + \frac{\partial u_j}{\partial x_i}\right) \quad (5)$$

In these equations, P_k represents the generation of turbulence kinetic energy due to the mean velocity gradients, calculated in same manner as standard k-ε model P_b is the generation of turbulence kinetic energy due to buoyancy, calculated in same way as standard k-ε model (Internet-2, 2014). And turbulence model constants are below:

$C_{1\epsilon}$ = 1.44, C_2 = 1.9, σ_k = 1.0, σ_ϵ = 1.2
σ_k : TKE Prandtl Number
σ_ϵ : TDR Prandtl Number (Fluent Inc., 2006)

MODEL GEOMETRY

The main aim of this study is to investigate and compare airfoils on VAWT, and these airfoils, NACA0021, NACA0015, NACA5520 and Clark-Y, are illustrated in Figure 3. NACA0021 was used to validate numerical solution methodology by study of Castelli et al. The other airfoils examined were selected to investigate the effects of thickness and camber position and amount on the performance criteria.

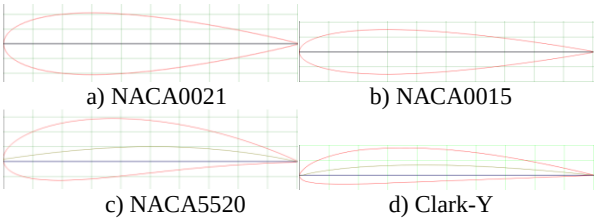

Figure 3. Considered airfoils in the study (Internet-1).

Wind Tunnel Sub-Grid

Darrieus rotor was placed in a visionary wind tunnel area of 80 m high and 1 m deep. Cross section area of the wind tunnel is 80 m^2 (A_{tunnel}) so that blockage effects should not be important, as was in the study by Castelli et al (2011). The Darrieus rotor's diameter and height are of 1.03 m and 1 m, respectively, so the cross section area of the Darrieus rotor is 1.03 m^2 (A_{rotor}). And the solid blockage factor defined by (6):

$$\beta = 0.25 \frac{A_{rotor}}{A_{tunnel}} \quad (6)$$

β has value of 0.32% ensuring the possibility to use numerical data with a simple blockage factor correction. Solution model and boundary conditions have been placed, as shown in Fig. 4.

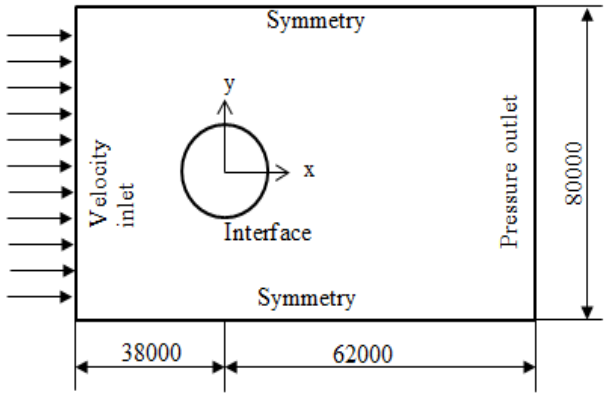

Figure 4. Main dimensions of the wind tunnel sub-grid area.

The main geometrical features of the tested rotor are summarized in Table 1. The solidity parameter σ is defined as A_{blades}/A_{rotor}.

Table 1: Main geometrical features of the tested model.

D_{rotor}	1.30m
H_{rotor}	1.00m (2D simulation)
N [-]	3
Blade Profile	NACA0021, NACA0015, NACA5520 and Clark-Y
c [m]	0.0858
Spoke-blade connection	0.25c
σ	0.5

- Two symmetry boundary conditions were used for the side walls. The circumference around the circular opening, centered on the turbine rotational axis, was set as an interface, thus ensuring the continuity in the flow field.
- A rectangular outer zone, determining the overall calculation domain, with a circular opening centered on the turbine rotational axis, which was identified as Wind Tunnel sub-grid, fixed, as shown Fig. 4.

An unstructured and stationary grid was chosen for the Wind Tunnel sub-grid, in order to reduce solution time to prepare the CFD simulations. The Wind Tunnel sub-grid has 18630 nodes (without Rotor sub-grid and control circles).

Rotor Sub-Grid

A circular inner zone, which was identified as rotor sub-grid, rotating with rotor angular velocity ω, as shown in Fig. 2. The Rotor sub-grid is the fluid area simulating the revolution of the wind turbine and is therefore characterized by a moving mesh, rotating at the same angular velocity of the turbine. Its location coincides exactly with the circular opening inside the wind tunnel sub-grid area and centered on the turbine rotational axis. Fig. 5 shows the main dimensions and the boundary conditions of the Rotor sub-grid area. It is good engineering method to ensure that the mesh on both sides of the interface (Rotor sub-grid and Wind Tunnel sub-grid areas) has approximately the same characteristic cell size in order to obtain faster convergence (Fluent Inc., 2006).

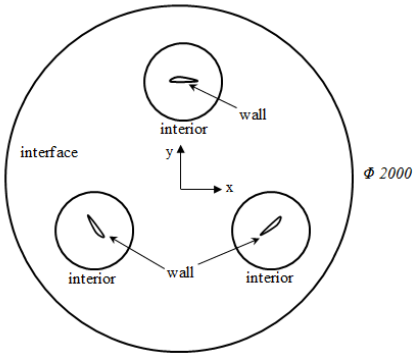

Figure 5. Schema of rotor sub-grid area.

The Control Circle

The control circle was placed in rotors the diameter of which is 1.03 m, and pressure center of Blade-1 was set at 0.25c. The diameters of the control circles are 400 mm as shown in Fig 6., and the chord distance of airfoil is 85.8 mm as given in Table 1.

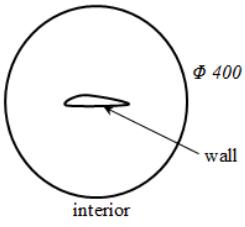

Figure 6. The control circle

Grid Independence

Grid size is another parameter affecting accuracy of the numerical solution methodology. At the beginning of the numerical studies, grid independence should be ensured for both obtaining the most accurate results and saving solution time. In this scope, three different grid models were examined to prove mesh independence of

the numerical solution. Fig. 7-10 illustrate the grid structures for wind tunnel, rotor, control circle and wall of blade boundary, respectively. It has been obtained grid independence with Model-2 that has a cell size of 560,000 elements (Fig. 11). Since mesh number rather affects the time of solution, determining the one that does not affect the solutions and has lower mesh number is logical. Model-1 and Model-2 is similar to each other as regards the torque values, but model-3 differs from them (Fig 12). So model-2 has been chosen for the analysis. The present simulations were worked by using a computer with 8 CPU, 2.93 GHz, 16 GB RAM, and required a total CPU time of about 3 days for each simulation.

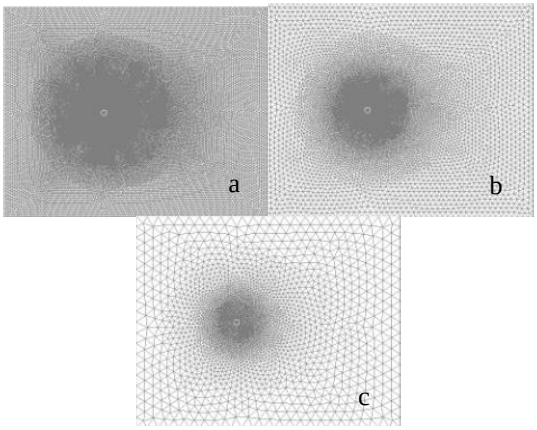

Figure 7. Wind tunnel sub-grid grid models [a) Model-1, b) Model-2, c)Model-3].

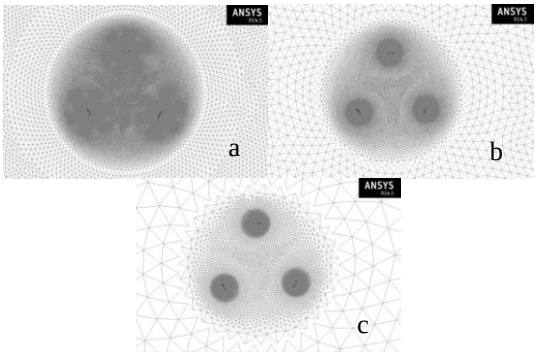

Figure 8. Rotor sub-grid grid models [a) Model-1, b) Model-2, c) Model-3].

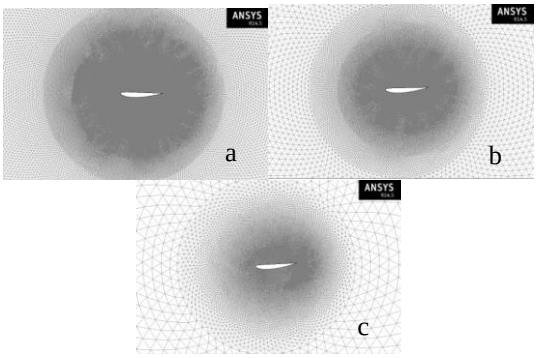

Figure 9. Control Circle Sub-Grid Grid Models [a) Model-1, b) Model-2, c) Model-3].

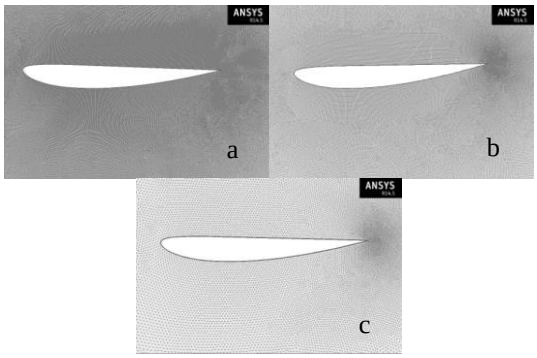

Figure 10. Blade boundary sub-grid grid models [a) Model-1, b) Model-2 c) Model-3].

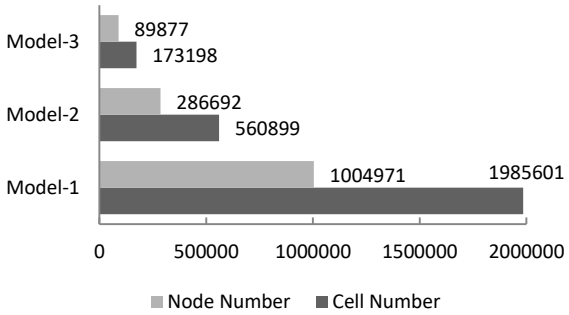

Figure 11. Node and Cell numbers of three different mesh models.

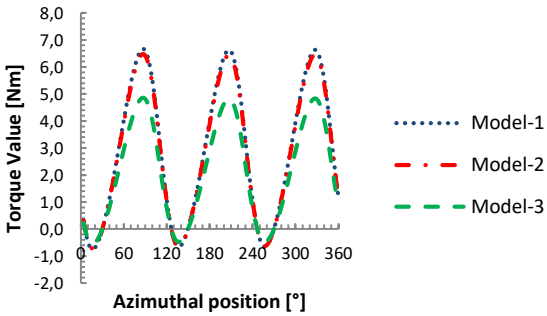

Figure 12. Grid independence.

RESULTS AND DISCUSSIONS

The calculated quantities were combined in order to obtain the performance parameters commonly used in the aerodynamic of wind turbines: the power coefficient (7) and the torque coefficient (8) evaluated as function of the dimensionless parameter Tip-Speed Ratio (9). Where A = 2RL is the frontal rotor area, R is the rotor radius and L is the rotor height, U is wind velocity, ω is angular velocity of rotor P is power that obtained from wind.

$$C_p = \frac{P}{\frac{1}{2}\rho A U^3} \tag{7}$$

$$C_T = \frac{T}{\frac{1}{2}\rho A R U^2} \tag{8}$$

$$TSR = \frac{\omega R}{U} \quad (9)$$

Calculated C_p values of NACA0021 were obtained between numerical and experimental NACA0021 study by Castelli et al. (2011). As can be seen in Fig. 13, the C_p curve of NACA0021 is also compared with the results from Castelli et al.'s study (2011)]. The calculated C_p values are consistent with the results given in the literature. As seen in this figure, the maximum C_p value was obtained about 2.5 tip speed ratio.

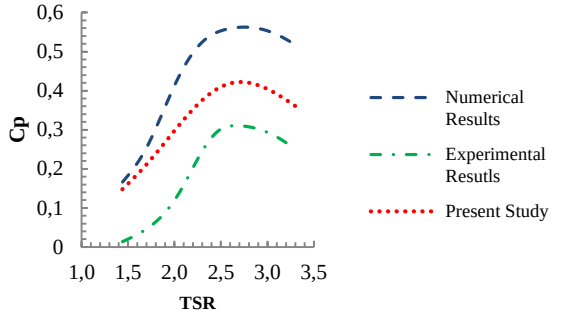

Figure 13. Power coefficient curves of numerical, experimental and validation of NACA0021 as a function of TSR (Tip Speed Ratio) (Castelli et al., 2011).

Figure 14 illustrates calculated C_p values versus the TSR value for NACA0021, NACA0015, NACA5520 and Clark-Y. As seen from this figure, the maximum C_p values of NACA0021, NACA0015, NACA5520 and Clark-Y are obtained at TSR=2.51, 2.64, 2.33 and 3.30, respectively. Scheurich et al. (2013) numerically invetstigated the effets of steady and unsteady flow conditions on a vertical axis wind turbine. They used NACA0015 as an airfoil and concluded that higest power coefficent value is near TSR number of 3 and rotor azimuthal position of nearly 90º , like present study. Due to dynamic stall at low TSR numbers, namely low rational speeds, obtained power from wind is less than high rational speeds as Frunzulica et al. (2013) stated. Although operation of VAWT at low tip speed ratios offers numerous noise and safety advantages even higher blade speed ratios suffer from dynamic stall that decreases their performance (Yen et al., 2013). Also, fluctuations in the dynamic stall at low TSR values can cause fatigue damage (Ferreiara et al., 2009).

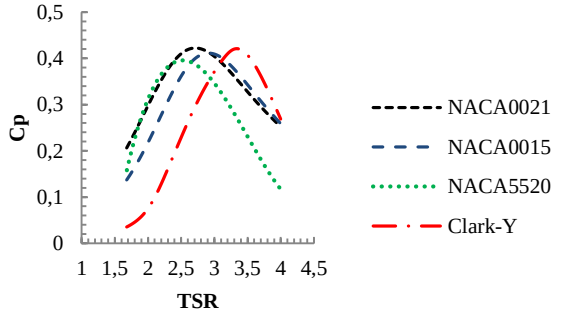

Figure 14. Power coefficient curves of of NACA0021, NACA0015, NACA5520 and Clark-Y as a function of TSR.

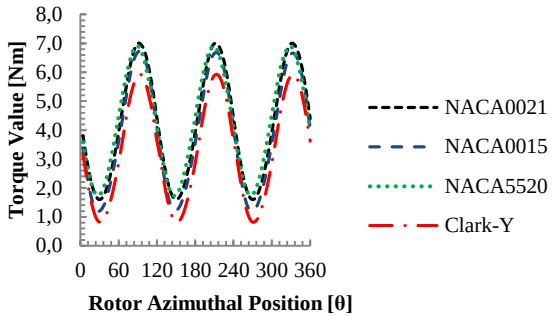

Figure 15. Torque Values as a Function of Rotor Azimuthal Position for NACA0021, NACA0015, NACA5520 and Clark-Y; TSR=2.51, 2.64, 2.33 and 3.30 frequently (average torque values is maximum for each ones).

As can be seen in Fig. 15, torque values recur at every 120° rotor azimuthal position. As the TSR increases, C_p curves of the airfoils begin to convergence. Furthermore, the maximum average torque values for each airfoils which depend on TSR numbers for NACA0021, NACA0015, NACA5520 and Clark-Y is 2.51, 2.64, 2.33 and 3.30 of TSR numbers, respectively, as given in Fig. 15. At high rotational speed, if TSR values are between 3 and 4, Clark-Y airfoil could be used. However, at low rotational speeds, NACA0021 or NACA5520 airfoil should be chosen as its initial movement is superior to others.

When these three airfoils are compared with each other, as the thickness of the blade airfoil increases, C_p value is elevated at lower TSR numbers from peak point. The increase in the thickness of airfoil plays a role in increasing the torque value due to fact that the effect of lift force provides greater moment. At the same time, drag effect of wind becomes higher at high rotational speeds due to the increase in the thickness of airfoil and it provides more decrement of power. However, the parameter is not only thickness; there are also camber, position of max camber, cord distance, rotor diameter and height, etc.

The cause of Cp curves starts to decrease at a specific TSR value is the rising impact of blade translational speed near the other blade flow field. So there is an optimum working condition of each airfoil at a specific TSR value and rotor azimuthal position. Fig. 15 illustrates that each airfoil has a position where maximum torque is obtained at the about 88°-92° of rotor azimuthal position. On working vertical axis wind turbines, unsteady fluctuation may occur and affect the performance of wind turbines. About this subject, the results of Wekesa et al. (2014) study derived from in the numerical analysis show that, within fluctuating free-stream wind conditions, thicker airfoils are desirable. They also concluded that unsteady power coefficient variation cross the steady CP curve as the wind fluctuates for both blade thickness. Overall maximum unsteady Cp of VAWT with thicker blades reveals positive deviations if the tip speed ratio is slightly

higher than that of the steady maximum Cp, while thinner blades maximum Cp marginally drops from the steady maximum Cp for the same λ range.

Both positive and negative torque coefficient can be obtained depending on position of blades. Fig. 16, 17, 18 and 19 show torque coefficient each blades of each airfoils. Torque coefficient is calculated by using equation (9). At minimum TSR number of 1.68, the total torque coefficient is maximum on NACA5520, but the total torque coefficient is minimum value on Clark-Y due to dynamic stall at some azimuthal positions. For Clark-Y, the torque coefficent show irregularity at some rotor azimuthal positions. At TSR number of 2.33 (as in Fig. 16, 17, 18, and 19), total torque value of NACA0021 and NACA0015 is higher than that of each blades; however, total torque value of NACA5520 and Clark-y is lower than that of each blades, due to more dynamic stall on asymmetric airfoils. The torque value can have suddenly negative and positive values nearby 12°, 132° and 252° rotor azimuthal positions. In adition to this, maximum torque values are obtained 92º, 212ºand 302º like Danao et al. (2014) numerically investigated NACA0022 on a small-scale vertical axis wind turbine. Fig. 20 is given to show torque values of each airfoil at constant 2.64 of TSR number in a circular diagram type. In addition, they concluded that all capturing the maximum torque was accurately predicted around θ=80°.When one of the blades is at azimuthal position of maximum torque value, other blades provide little support to torque value.

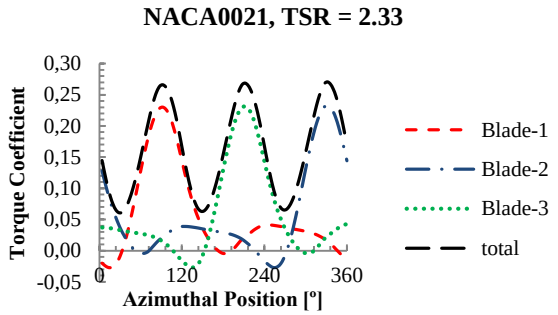

Figure 16. Torque coefficient values of each blades and total NACA0021, TSR=2.33.

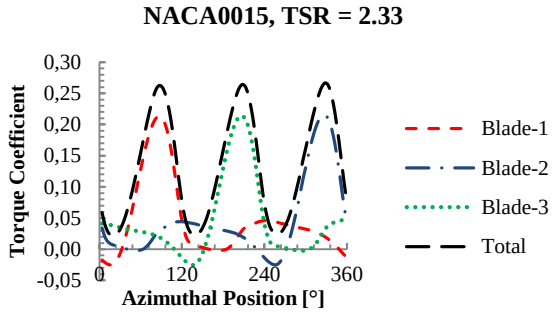

Figure 17. Torque coefficient values of each blades and total on NACA0015, TSR=2.33.

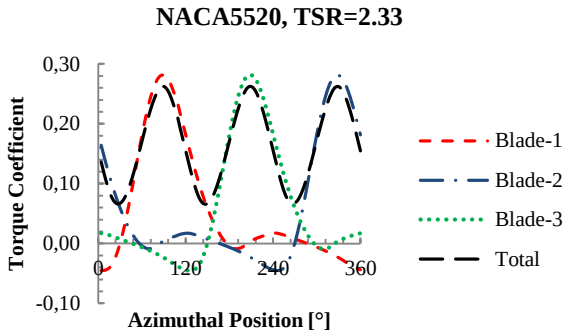

Figure 18. Torque coefficient values of each blades and total on NACA5520, TSR=2.33.

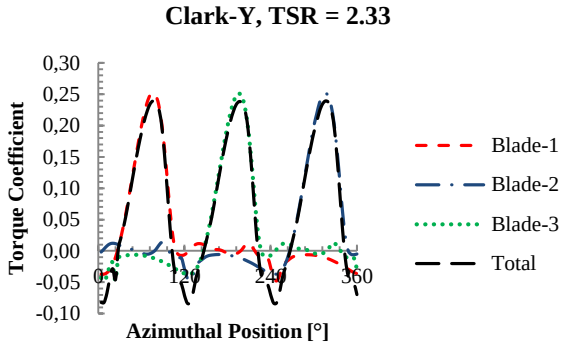

Figure 19. Torque coefficient values of each blades and total Clark-Y, TSR=2.33.

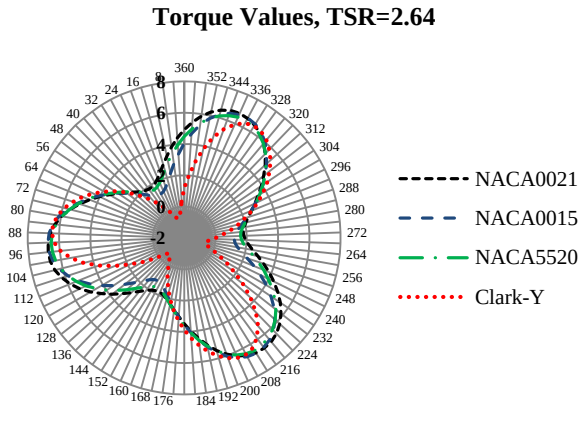

Figure 20. Torque values of the airfoils at each airfoil rotor azimuthal positions for TSR = 2.64.

Fig. 21 and Fig. 22 illustrate that; successively, velocity and total pressure contours for three blades of NACA0021, NACA0015, NACA5520 and Clark-Y at 92º rotor azimuthal position at 1.68 of TSR number; and Fig 23 and 24 illustrate that of 2.64 of TSR number.

The cause of decreasing of torque value is that dynamic stall can be seen especially for Blade-1 of NACA0015 and Clark-Y. However, the dynamic stalls do not occur at 2.64 of TSR number at same rotor azimuthal position, so torque value is higher than 1.68 of TSR number; as Yen et al. (2013) cited.

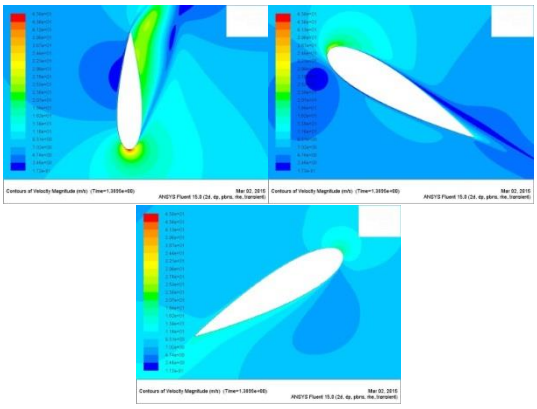

a) NACA0021

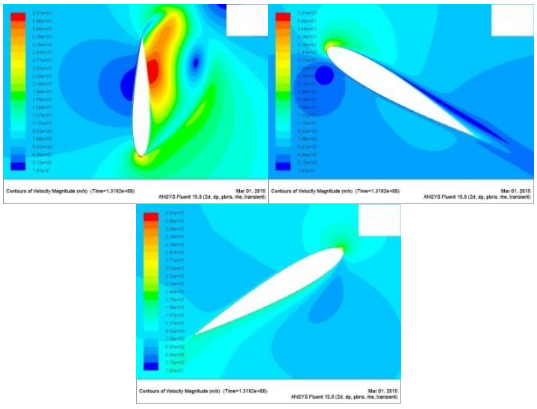

b) NACA0015

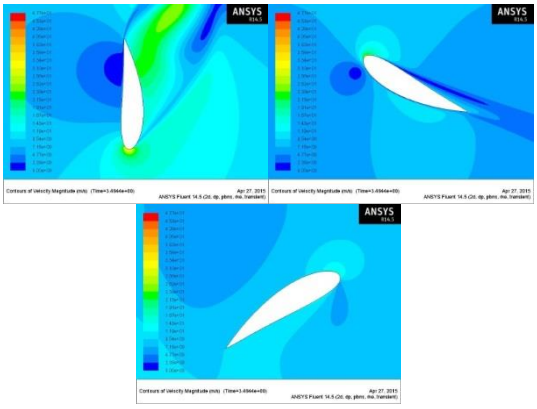

c) NACA5520

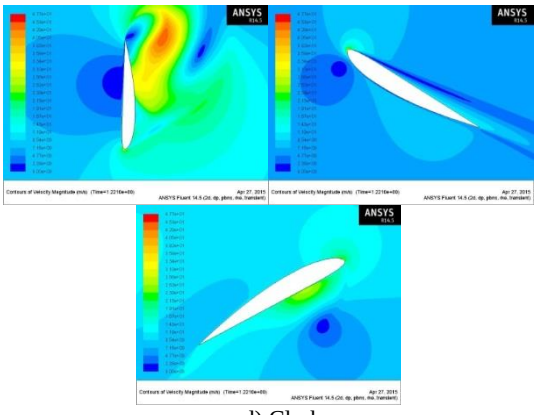

d) Clark-y

Figure 21. Velocity contours for each airfoils (Blade-1, 2 and 3 respectively) at 92º rotor azimuthal position and TSR=1.68.

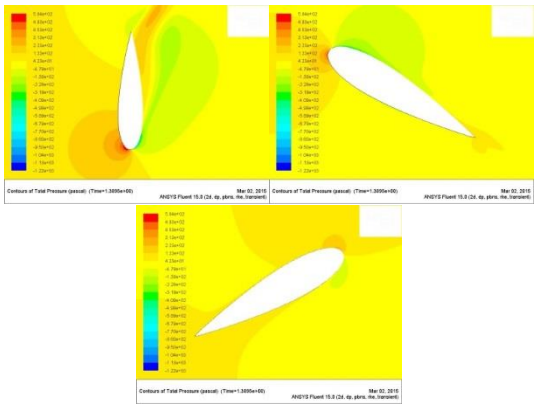

a) NACA0021

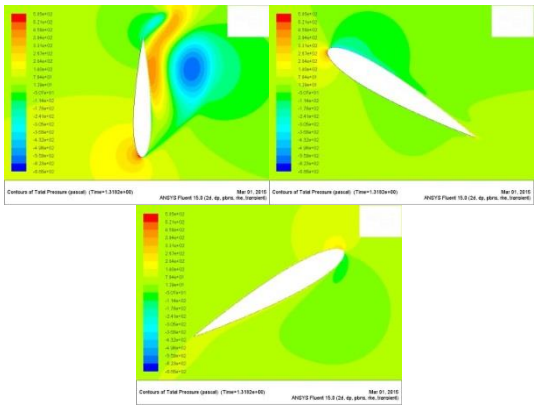

b) NACA0015

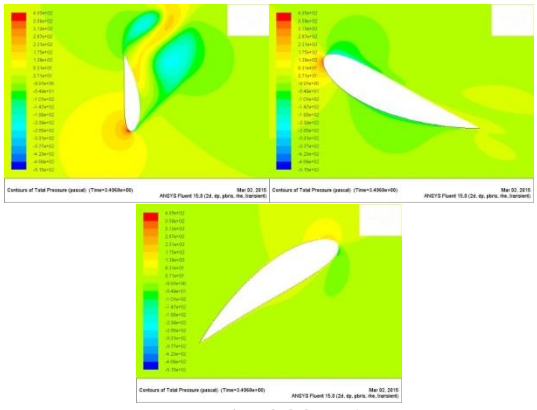

c) NACA5520

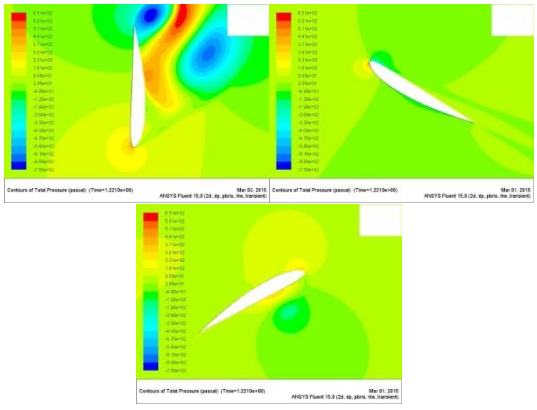

d) Clark-y

Figure 22. Total pressure contours for each airfoils (Blade-1, 2 and 3 respectively) at 92º rotor azimuthal position and TSR=1.68.

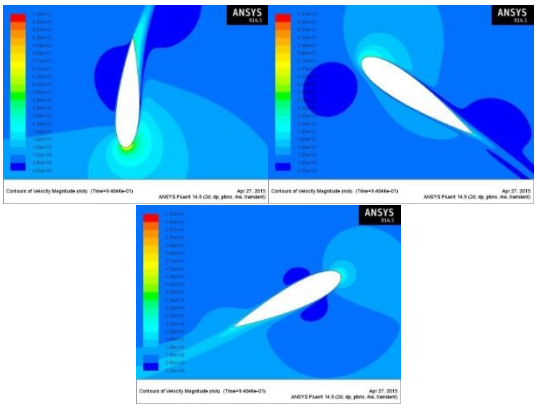

a) NACA0021

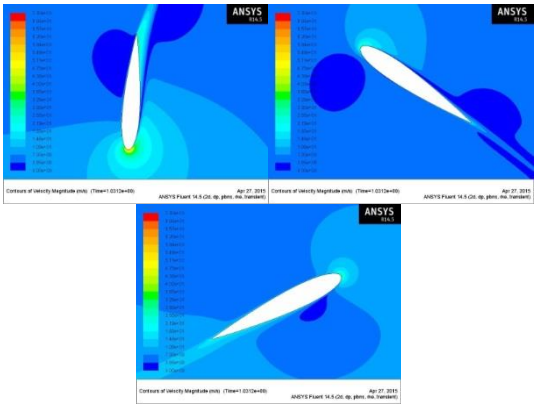

b) NACA0015

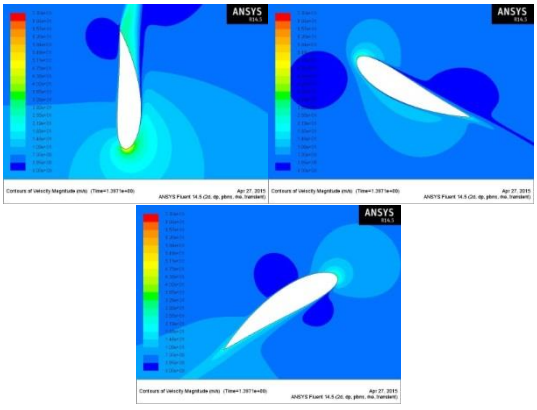

c) NACA5520

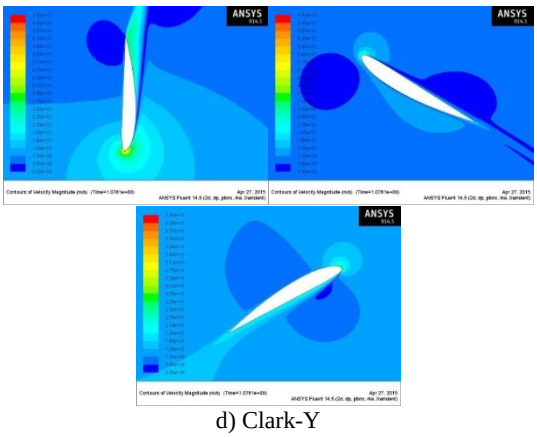

d) Clark-Y

Fiureg 23. Velocity contours for each airfoils (Blade-1, 2 and 3 respectively) at 92º rotor azimuthal position and TSR=2.64.

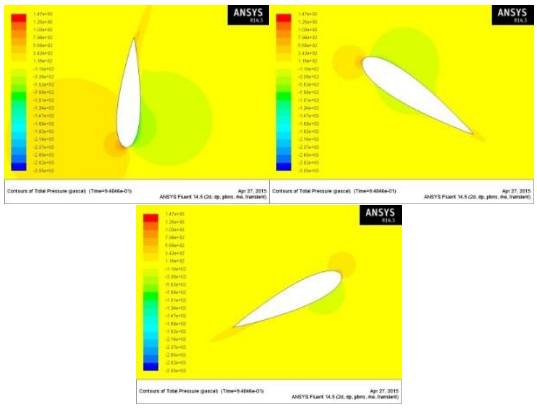

a) NACA0021

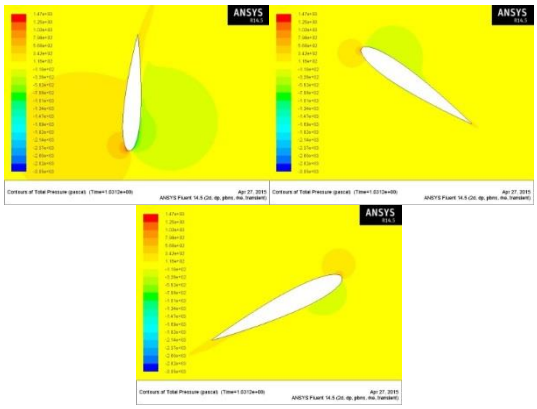

b) NACA0015

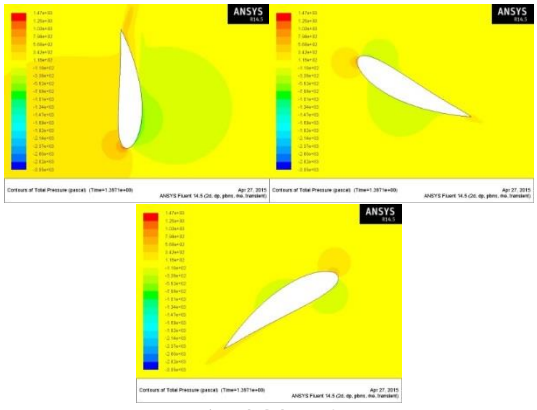

c) NACA5520

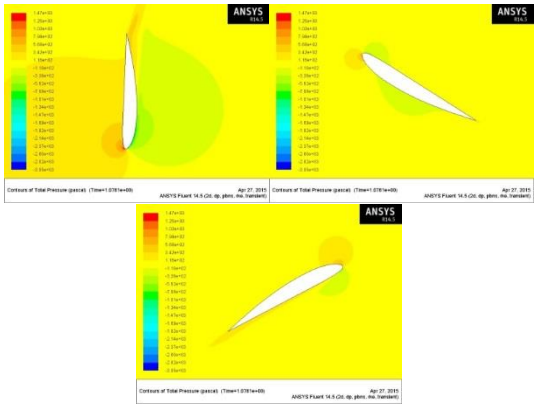

d) Clark-Y

Figure 24. Total pressure contours for each airfoils (Blade-1, 2 and 3 respectively) at 92º rotor azimuthal position and TSR=2.64.

CONCLUSION

Choosing the type of the airfoil is a parameter in designing wind turbines, and turbine operating conditions must be determined. In this context, all of the examined airfoils can be utilized, but rotating speed depends on wind velocity, and azimuthal positions of the blades must be considered before planning the turbine design.

- As a result of the air force applied to the wings, maximum torque values have been determined in the azimuthal positions of nearly 90º.
- As decreasing the thickness of airfoil, peak points of the C_p curves is occurring higher TSR numbers.
- Turbulent effect suddenly increases at some TSR numbers, and it causes torque values to have a peak. However, when the rotating speed increases, the effect of turbulent has been reduced. And so each airfoil almost begins to show the same aerodynamic characteristic.
- If NACA0021, NACA0015, NACA5520 and Clark-Y are compared on a Darrieus vertical axis wind turbine, Naca0021 is more efficient than others at average TSR numbers; but at least Clark-Y is more effective for TSR values that bigger than 3.00, and NACA5520 is better for first movement.
- At low TSR numbers, total torque value of symmetric airfoils, like NACA0021 and NACA0015, is higher than that of each blades; however, total torque value of asymmetric airfoils, like NACA5520 and Clark-y; is lower than that of each blades, due to greater dynamic stall on asymmetric airfoils.
- Especially at low TSR numbers, NACA5520 can be employed for first movement due to fact that the gradient of power coefficient of it is high. In other words, it reaches to the peak point of the C_p value faster than other airfoils at low TSR numbers.

ACKNOWLEDGEMENTS

This study was sponsored by Erciyes University and the Ministry of Science, Industry and Technology, Republic of Turkey (SAN-TEZ project code number of 01354.STZ.2012-1).

REFERENCES

Bergey B, *Wind Energy History*, Windpower.com, Oklahoma, 1997.

Bhutta MMA, Hayat N, Farooq AU, Ali Z, Jamil SR, Hussain Z. Vertical axis wind turbine – A review of various configurations and design techniques, *Renewable and Sustainable Energy Reviews*, 2012; 16: 1926-1939.

Castelli MR, Englaro A, Benini E. The Darrieus wind turbine: Proposal for a new performance prediction model based on CFD, *Energy*, 2011; 36: 4919-4934.

Ferreiara CJS, van Zuijlen A, Bijl H, van Bussel G, van Kuik G. Simulating dynamic stall in a two-dimensional vertical-axis wind turbine: verification and validation with particle image velocimetry data, *Wind Energy*, 2009; 13: 1-17.

Fluent Inc., *Fluent User's Manual*. pp. 52, 54, 59, 71, 143, 2006.

Frunzulica F, Dumitrescu H, Dumitrache A. A numerical investigation on the dynamic stall of a vertical axis wind turbine, *Proc. Appl. Math. Mech*, 2013; 13: 295-296.

Guleren MK, Demir S. Performance analysis of different airfoils for wind turbine blades at low angles of attack, *Journal of Thermal Science and Technology*, 2011; 31-2: 51-59.

Horikiri K, Aerodynamics of wind turbines, *A Thesis Submitted For The Degree Of Master Of Philosophy To The University Of London*, London, 2011.

Howell R, Qin N, Edwards J, Durrani N. Wind tunnel and numerical study of a small vertical axis wind turbine, Renewable Energy, 2010; 35: 412-422.

Internet-1, 2014, Airfoil Tools, *Airfoil 4 Digit Generator*, http://airfoiltools.com/airfoil/naca4digit

Internet-2, 2014, CFD-Online, *k-epsilon Turbulence Model*, http://www.cfd-online.com/Wiki/Realisable_k-epsilon_model

Jin X, Zhao G, Gao K, Ju W. Darrieus vertical axis wind türbine: Basic research methods. *Renewable and Sustainable Energy Reviews*, 2015; 42: 212-225.

Kishore RA, Priya S. Design and experimental verification of a high efficiency small wind energy portable turbine (SWEPT), *Journal of Wind Engineering and Industrial Aerodynamics*, 2013; 118 : 12–19.

Nini M, Motta V, Bindolino G, Guardone A. Three-dimensional simulation of a complete Vertical Axis Wind Turbine using overlapping grids, *Journal of Computational and Applied Mathematics*, 2014; 270: 78–87.

Nobile R, Vahdati M, Barlow JF, CrookAM. Unsteady flow simulation of a vertical axis augmented wind turbine: A two-dimensional study, *Journal of Wind Engineering and Industrial Aerodynamics*, 2014; 125: 168–179.

Scheurich F, Brown RE. Modelling the aerodynamics of vertical-axis wind turbines in unsteady wind conditions, *Wind Energy*, 2013; 16: 91-107.

Saeidi D, Sedaghat A, Alamdari P, Alemrajabi AA. Aerodynamic design and economical evaluation of site specific small vertical axis wind turbines. *Applied Energy*. 2013; 101 : 765-775.

Tummala A, Velamati RK, Sinha DK, Indraha V, Krishna VH. A review on small scale wind turbines, Renewable and Sustainable Energy Reviews, 2016; 58: 1351-1371.

Wekesa DW, Wang C, Wei Y, Danao LAM. Influence of operating conditions on unsteady wind performance of vertical axis wind turbines operating within a fluctuating free-stream: A numerical study, *Journal of Wind Engineering and Industrial Aerodynamics*, 2014; 135: 76-89.

Tjiu W, Marnoto T, Mat S, Ruslan MH and Sopian K. Darrieus vertical axis wind turbine for power generation I: Assessment of Darrieus VAWT configurations, *Renewable Energy*, 2015; 75: 50-67.

Yan L, Yuan C, Yongjun H, Shengmao L, Kotaro T. Numerical simulation on the aerodynamic effects of blade icing on small scale Straight-bladed VAWT, Harbin, *Physics Procedia*, 2012; 24: 774-780.

Yen J, Ahmed NA. Enhancing vertical axis wind turbine by dynamic stall control using synthetic jets, *Journal of Wind Engineering and Industrial Aerodynamics*, 2013; 114: 12-17.